

SVDNet for Pedestrian Retrieval

Yifan Sun[†], Liang Zheng[‡], Weijian Deng[§], Shengjin Wang[†]

[†]Tsinghua University

[‡]University of Technology Sydney

[§]University of Chinese Academy of Sciences

sunyf15@mails.tsinghua.edu.cn

Abstract

This paper proposes the SVDNet for retrieval problems, with focus on the application of person re-identification (re-ID). We view the weight matrix W as a set of projection vectors or basis. It is observed that the weight vectors are usually highly-correlated. This problem leads correlations among entries of the FC descriptor, and compromises the retrieval performance based on the Euclidean distance. To alleviate the correlation problem, this paper proposes to decorrelate the learned weight vectors using singular vector decomposition (SVD). Specifically, we design a novel training strategy with the “restraint and relaxation iteration” (RRI) scheme. We conduct experiments on the Market-1501, CUHK03, and Duke datasets, and show that RRI effectively reduces the correlation among the projection vectors and significantly improves the re-ID accuracy. On the Market-1501 dataset, for instance, rank-1 accuracy is improved from 55.2% to 80.5% for CaffeNet, and from 73.8% to 83.1% for ResNet-50.

1. Introduction

This paper considers the problem of pedestrian retrieval, also called person re-identification (re-ID). This task aims at retrieving images containing the same person to the query.

Person re-ID is different from image classification in that the training and testing sets contain entirely different classes. So a popular deep learning baseline consists in 1) training a classification deep model on the training set, 2) extracting image descriptors using the fully-connected (FC) layer for the query and gallery images, and 3) computing similarities based on Euclidean distance before returning the sorted list [31, 29, 24, 9].

Our work is motivated by the observation that after training a CNN model for classification, the weight vectors within a certain FC layer are highly correlated. We infer this problem arises mainly due to two reasons. The first reason

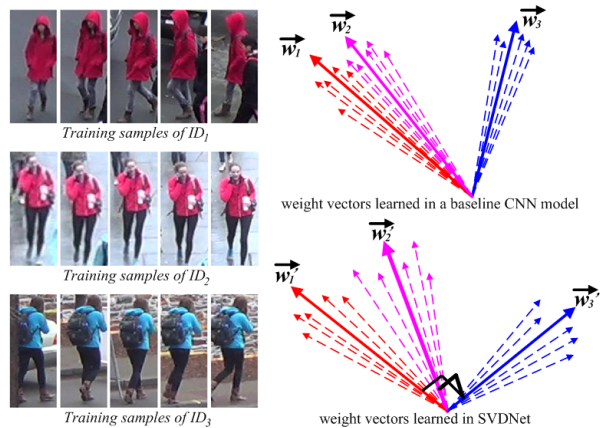


Figure 1. A cartoon illustration of the correlation among weight vectors and the cause. The weight vectors is contained in the last fully connected layer, e.g., FC8 layer of CaffeNet [11] or FC layer of ResNet-50 [10]. There are three training IDs in red, pink and blue clothes from the Duke dataset [16]. Under the baseline setting, some learned weight vectors are highly correlated. The motivation of SVDNet, is to enforce orthogonality to the weight matrix.

is related to the uneven distribution of training samples, especially when focusing on the last FC layer. Consider the neuron on the last FC layer, whose output represents the similarity between the input and the corresponding training identity. If there exist two inherently similar training identities, the weight vectors contained in the corresponding neurons are also highly correlated, as the red and the pink vector shown in Fig. 1. The second reason is that in a CNN-based classification model, there exists few, if any, orthogonalization items. So the learned weight vectors may be naturally correlated.

Correlation among weight vectors of the FC layer compromises the FC descriptor significantly when we consider the retrieval task under the Euclidean distance. In fact, a critical assumption of using Euclidean distance (or equivalently the cosine distance after ℓ_2 -normalization) for

retrieval is that the entries in the feature vector should be possibly independent. However, when the weight vectors are correlated, the FC descriptor projection on these weight vectors of the output of a previous CNN layer will have correlated entries. For example, if many weight vectors are highly correlated, the FC descriptor of an image will have very similar values in the corresponding entries, which will dominate the Euclidean distance, leading to poor ranking results (*e.g.*, the projection values along the red and the pink vector are close and might eclipse the projection values along the blue vector as in Fig.1). It is of vital importance to reduce the redundancy in the FC descriptor to make it work under the Euclidean distance.

To address the correlation problem, this paper proposes SVDNet, which features an FC layer containing decorrelated weight vectors as well as a novel three-step training procedure. In the first step, the weight matrix undergoes the singular vector decomposition (SVD) and is replaced by the product of the left unary matrix and the singular value matrix. Second, we keep the orthogonalized weight matrix fixed and only fine-tune the rest layers. Third, the weight matrix is set unfrozen and the whole network is trained for overall optimization. The three steps are iterated to perform an alternating rhythm of “restraint and relaxation” to enforce orthogonality. Experimental results on three large-scale re-ID datasets demonstrate significant accuracy improvement over the baseline network, and our results are on par with the state of the art.

2. Related Work

Deep learning for person re-ID. In person re-ID, deep learning methods can be classified into two classes: similarity learning and representation learning. The former is also called deep metric learning, in which image pairs or triplets are used as input to the network [23, 22, 1, 12, 5]. In the two early works, Yi *et al.* [27] and Li *et al.* [12] use image pairs and inject part priors into the learning process. In later works, Varior *et al.* [23] incorporate long short-term memory (LSTM) modules into a siamese network. LSTMs process image parts sequentially so that the spatial connections can be memorized to enhance the discriminative ability of the deep features. Varior *et al.* [22] insert a gating function after each convolutional layer to capture effective subtle patterns between image pairs. The above-mentioned methods are effective in learning image similarities in an adaptive manner, but may have efficiency problems under large-scale galleries.

The second type of CNN-based re-ID methods focus on feature learning, which categorizes the training samples into pre-defined classes and the FC descriptor is used for retrieval [31, 19, 24]. In [31, 32], the classification CNN model is fine-tuned using either the video frames or image bounding boxes to learn a discriminative embedding for

pedestrian retrieval. Xiao *et al.* [24] propose learning generic feature representations from multiple re-ID datasets jointly. To deal with spatial misalignment, Zheng *et al.* [29] propose the PoseBox structure similar to the pictorial structure [6] to learn pose invariant embeddings. To take advantage of both the feature learning and similarity learning, Zheng *et al.* [33] and Geng *et al.* [9] combine the contrastive loss and the identification loss to improve the discriminative ability of the learned feature embedding, following the success in face verification [20]. This paper adopts the classification mode, which is shown to produce competitive accuracy without losing efficiency potentials.

PCANet and truncated SVD for CNN. Here we clarify the difference between SVDNet and several “look-alike” works. In [3], Chan *et al.* propose the PCANet for image classification. It is featured with cascaded principal component analysis (PCA) filters. PCANet is related to SVDNet in that it also learns orthogonal projection directions to produce the filters. **The proposed SVDNet differs from PCANet in two major aspects.** First, SVDNet performs SVD on the weight matrix of CNN, while PCANet performs PCA on the raw data and feature. Second, the filters in PCANet are learned in an unsupervised manner, which does not rely on back propagation as in the case of SVDNet. In fact, SVDNet manages a stronger connection between CNN and SVD. SVDNet’s parameters are learned through back propagation and decorrelated iteratively using SVD.

Truncated SVD [7, 26] is widely used for the purpose of CNN compression, as well as in many other domains. SVDNet departs from it in two aspects. First, truncated SVD decomposes the weight matrix in FC layers and reconstructs it with several dominant singular vectors and values. SVDNet does not reconstruct the weight matrix but replaces it with an orthogonal matrix, which is the product of the left unary matrix and the singular value matrix. Second, Truncated SVD reduces the model size and testing time at the cost of acceptable precision loss, while SVDNet significantly improves the retrieval accuracy without impact on the model size.

Orthogonality in the weight matrix. We note a concurrent work [25] which also aims to orthogonalize the CNN filters, yet our work is different from [25]. In [25], the regularization effect of orthogonalization benefits the back-propagation of very deep networks, thus improving the classification accuracy. The regularization proposed in [25] may not directly benefit the embedding learning process. But in this paper, orthogonalization is used to generate decorrelated descriptors suitable for retrieval. Our network may not be suitable for improving classification.

3. Proposed Method

In this section, we will describe the structure of SVDNet, its training strategy, and its working mechanism in Section

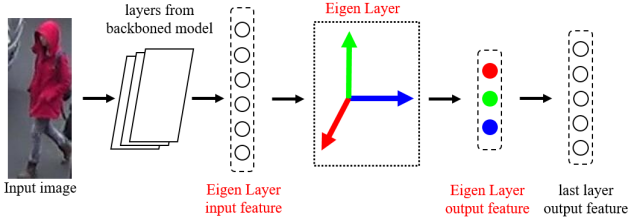


Figure 2. The architecture of SVDNet. SVDNet contains an Eigen Layer before the last FC layer of the backbone model. The weight vectors of the Eigen Layers are expected to be orthogonal to each other. In testing, either the *Eigen Layer input feature* or the *Eigen Layer output feature* is employed for retrieval.

3.1, Section 3.2 and Section 3.3, respectively.

3.1. Architecture

SVDNet mostly follows the backbone networks, *e.g.*, CaffeNet and ResNet-50. The only difference is that SVDNet uses an Eigen Layer as the second last FC layer as shown in Fig. 2. the Eigen Layer contains an orthogonal weight matrix and is a linear layer with no bias. The reason for not including bias is that the bias will disrupt the learned orthogonality. In fact, our preliminary experiments indicate that adding the ReLU activation and the bias term slightly compromises the re-ID performance, so we choose to implement the Eigen Layer based on a linear layer. The reason for positioning Eigen Layer at the second last FC layer, rather than the last one is that the model fails to converge when orthogonality is enforced on the last FC layer in our preliminary experiments, which might be because the correlation of weight vectors in the last FC layer is determined by the sample distribution, as explained in the introduction.

During training, the input feature from a previous layer is passed through the Eigen Layer. Its projections on the weight vectors form the output feature of the Eigen Layer, which is fully connected to the last layer of c -dim, where c denotes the number of training classes.

During testing, we extract the learned embeddings for the query and gallery images. In this step, we can use either the Eigen Layer input feature or the Eigen Layer output feature as shown in Fig. 2. Our experiment suggests that the two features have similar performance, and that the input feature is slightly superior.

3.2. Training SVDNet

The algorithm of training SVDNet is presented in Alg. 1. We first briefly introduce Step 0 and then describe the Restraint and Relaxation Iteration (RRI) (Step 1, 2, 3).

Step 0. We first add a linear layer to the network. For CaffeNet, it replaces FC7; for ResNet-50, it is inserted between Pool5 and FC. Then, the network is fine-tuned till

Algorithm 1: Training SVDNet

```

0. Add the eigen layer and fine-tune the network.
for  $t \leftarrow 1$  to  $T$  do
  1. Decorrelation: Decompose  $W$  with SVD
    decomposition, and then update it:  $W \leftarrow US$ 
  2. Restraint: Fine-tune the network with the eigen
    Layer frozen
  3. Relaxation: Fine-tune the network with the
    eigen Layer unfrozen
end

```

convergence. Note that after Step 0, the weight vectors in the Eigen layer are highly correlated. In the experiment, we will present the re-ID performance of the CNN model after Step 0. Various dimensions of the Eigen Layer output feature will be evaluated.

Restraint and Relaxation Iteration (RRI). It is the key procedure in training SVDNet. Three steps are involved.

- **Decorrelation.** W is decomposed with SVD: $W = USV^T$ and then replaced with US . This step decorrelates W , so that the weight vectors are orthogonal.
- **Restraint.** The backbone model is fine-tuned till convergence, but the Eigen Layer is *frozen*.
- **Relaxation.** The fine-tuning goes on for some more epochs with Eigen Layer *unfrozen*.

After Step 1 and Step 2, the weight vectors are orthogonal, *i.e.*, in an eigen state. But after Step 3, *i.e.*, Relaxation training, W shifts away from the eigen state. So the training procedure enters another iteration of “Restraint and Relaxation”.

As simple as it is, the mechanism behind the method is interesting. We will try to provide insight into the mechanism in the Section 3.3. During all the analysis involved, CaffeNet pre-trained on ImageNet is chosen as the backbone.

3.3. Mechanism Study

Correlation Diagnosing. The correlation between two weight vectors can be easily evaluated employing the correlation coefficient. However, so far as we know, there lacks a common evaluation protocol for diagnosing the overall correlation problem of a vector set. We propose an

evaluation protocol as follows. Assume

$$\begin{aligned}
 G = W^T W &= \begin{bmatrix} w_1^T w_1 & w_1^T w_2 & \cdots & w_1^T w_k \\ w_2^T w_1 & w_2^T w_2 & \cdots & w_2^T w_k \\ \vdots & \vdots & \ddots & \vdots \\ w_k^T w_1 & w_k^T w_2 & \cdots & w_k^T w_k \end{bmatrix} \\
 &= \begin{bmatrix} g_{11} & g_{12} & \cdots & g_{1k} \\ g_{21} & g_{22} & \cdots & g_{2k} \\ \vdots & \vdots & \ddots & \vdots \\ g_{k1} & g_{k2} & \cdots & g_{kk} \end{bmatrix} \quad (1)
 \end{aligned}$$

where G is the gram matrix of W . Then we define S to evaluate the extent of correlation between column vectors of W :

$$S(W) = \frac{\sum_{i=1}^k g_{ii}}{\sum_{i=1}^k \sum_{j=1}^k |g_{ij}|} \quad (2)$$

We can find that S achieves the largest value 1 only when W is an orthogonal matrix. When fine-tuning directly from CaffeNet, $S(FC7) = 0.0072$, indicating that the weight vectors of the FC7 layer are highly correlated. As we will show in Section 4.5, S is a critical indicator to determine the convergence of RRI.

Why SVD. This section explains why we use SVD to decorrelate weight vectors.

Our key idea is to decide a set of orthogonal projection directions based on what CNN has already learned from training set by itself. Intuitively, for a linear layer, a set of biases of the range space of W (i.e., linear subspace spanned by column vectors of W) will be a potential solution. However, there exist numerous sets of orthogonal biases. We decide to use the singular vectors of W as new projection directions and to weight projection results with the corresponding singular values. That is to replace $W = USV^T$ with $NW = US$. By doing this, **the discriminability of feature representation over the whole sample space will be maintained.** We make a mathematical proof as follows:

Assume that x_i and x_j are 2 arbitrary samples. \vec{h}_i and \vec{h}_j are the corresponding features before Eigen Layer. \vec{f}_i and \vec{f}_j are the features output from Eigen Layer. The Euclidean distance D_{ij} between feature representations of x_i and x_j is calculated by:

$$\begin{aligned}
 D_{ij} &= \|\vec{f}_i - \vec{f}_j\|_2 = \sqrt{(\vec{f}_i - \vec{f}_j)^T (\vec{f}_i - \vec{f}_j)} \\
 &= \sqrt{(\vec{h}_i - \vec{h}_j)^T W W^T (\vec{h}_i - \vec{h}_j)} \\
 &= \sqrt{(\vec{h}_i - \vec{h}_j)^T U S V^T V S^T U^T (\vec{h}_i - \vec{h}_j)} \quad (3)
 \end{aligned}$$

As long as V is a unit orthogonal matrix, it equals:

$$D_{ij} = \sqrt{(\vec{h}_i - \vec{h}_j)^T U S S^T U^T (\vec{h}_i - \vec{h}_j)} \quad (4)$$

Methods	<i>Orig</i>	<i>US</i>	<i>U</i>	<i>UV^T</i>	<i>QD</i>
R-1	63.57	63.57	61.67	61.67	61.58
mAP	39.21	39.21	37.14	37.14	37.26

Table 1. Performance of different methods of decorrelating W . Market-1501 and CaffeNet are used.

It is implicit that when changing $W = USV^T$ to $NW = US$, D_{ij} remains unchanged. Some other methods of decorrelation can be experimentally validated to degrade discriminability by some extent, as shown in Table 1. The settings are as follows:

- Using the original learned $W = USV^T$ (denoted by *Orig*);
- Updating W with $NW = US$ (denoted by *US*);
- Updating W with $NW = U$ (denoted by *U*);
- Updating W with $NW = UV^T$ (denoted by *UV^T*);
- Updating $W = QR$ (which means Q-R decomposition) with $NW = QD$, where D is the diagonal matrix extracted from the upper triangle matrix R (denoted by *QD*).

Four decorrelation methods from b) to e) all update the original W to be an orthogonal matrix NW containing a set of complete orthogonal biases of range space of W and thus preserve some knowledge learned by CNN. However, only updating W with $NW = US$ keeps the discriminability totally unchanged, while others considerably degrade the performance.

When does boosting happen. As proven, updating $W = USV^T$ with US does not bring an immediate boosting to discriminability, but keeps the discriminability exactly unchanged. However, after the decorrelation operation, the model has been pulled away from the optimal solution for fitting training data, and the classification loss on training set will decrease by a certain extent. A following retrain will fix it up, boosting the discriminability of feature representation. To be more specific, we conjecture that during retrain, the training loss is back propagated through the Eigen Layer, makes the model learn the feature before the Eigen Layer more adaptive to be projected to the orthogonal directions. For the same reason, the performance using input feature as well as using the output feature of Eigen Layer increases after the Restraint training. See the detailed evidence for the boosting procedure in Section 4.3.

Convergence Criteria for RRI. When to stop RRI is a non-trivial problem, especially in application. Note that in the Restraint step, the weight matrix W of the Eigen Layer is fixed, thus remains orthogonal. However, in the Relaxation stage, W shifts away from the eigen state and becomes nonorthogonal again. We employ Eq. 2 to evaluate the orthogonality of W after the Relaxation step and find that $S(W)$ increases as the iteration goes on. It indicates that the correlation among the weight vectors in W is

reduced step-by-step with RRI. So when $S(W)$ becomes stable, the model converges, and RRI stops.

Discussion on the RRI training strategy. Earlier in our work, a dilemma frustrates the approach to enforcing orthogonality on weight matrix: during the retrain following the decorrelation operation, if the weight matrix of Eigen Layer is fixed, the model will converge to a constrained optimal solution, while if the weight is free to be updated, the orthogonality will not be maintained. The proposed Restraint and Relaxation Iteration overcomes the dilemma. Interestingly, when educating a child, an alternating rhythm of relaxation and restraint is always encouraged.

4. Experiment

4.1. Datasets and Settings

Datasets. This paper uses three datasets for evaluation, *i.e.*, **Market-1501** [30], **CUHK03** [12] and **Duke** [17, 34]. The Market-1501 dataset contains 1,501 identities, 19,732 gallery images and 12,936 training images captured by 6 cameras. All the bounding boxes are generated by the DPM detector [8]. Most experiments relevant to mechanism study are carried out on Market-1501. The CUHK03 dataset contains 13,164 images of 1,467 identities. Each identity is observed by 2 cameras. CUHK03 offers both hand-labeled and DPM-detected bounding boxes, and we use the latter in this paper. 20 random train/test splits are performed, and the averaged results is reported. The Duke dataset is collected in [17] with 8 cameras and used for cross-camera tracking. We adopt its re-ID version benchmarked in [34]. The Duke dataset contains 1,404 identities (one half for training, and the others for testing), 16,522 training images, 2,228 queries, and 17,661 gallery images. For Market-1501 and Duke, we use the evaluation packages provided by [30] and [34], respectively.

For performance evaluation on all the 3 datasets, we use both the Cumulative Matching Characteristics (CMC) curve and the mean Average Precision (mAP).

General Settings. Experiments mainly contain 4 parts:

1) Performance Evaluation. Experiments are carried out to validate the significant performance improvement brought about by SVDNet. All the three datasets, *i.e.*, Market-1501, CUHK03 and Duke, are used.

2) Dimension comparison. The dimension of Eigen Layer’s output has relatively limited impact on the final performance of SVDNet. However, we find that for a model trained without enforcing orthogonality, a lower dimension improves the re-ID accuracy (under the premise that the model is capable to fit the training data). To our knowledge, this phenomenon has seldom been noticed in re-ID. So we treat the dimension as an important hyper-parameter and analyze its influence in Section 4.4.

The experiment is performed on Market-1501 with Caf-

feNet and ResNet-50.

3) RRI boosting procedure. We reveal the performance changes involved in the Restraint and Relaxation Iterations for training SVDNet. Experiments are performed on Market-1501 with CaffeNet and ResNet-50.

4) Comparison of decorrelation methods. We compare the final performances using 4 different decorrelation methods discussed in Section 3.3.

Backbones. We mainly use two networks pre-trained on ImageNet-1000 classification dataset as backbones, *i.e.*, CaffeNet [11] and ResNet-50 [10]. The former shares a very similar architecture with AlexNet. The latter has improved the state of the art on many vision tasks. When using CaffeNet as the backbone, we directly replace the original FC7 layer with the Eigen Layer, in case that one might argue that the performance gain is brought by deeper architecture. When using ResNet-50 as the backbone, we have to insert the Eigen Layer before the last FC layer because ResNet has no hidden FC layer and the influence of adding a layer into a 50-layer architecture can be neglected. In several experiments on Market-1501, we additionally use VGGNet [18] and a Tiny CaffeNet as backbones to demonstrate the effectiveness of SVDNet on different architectures. The Tiny CaffeNet is generated by reducing the FC6 and FC7 layers of CaffeNet to containing 1024 and 512 dimensions, respectively.

4.2. Implementation Details

Baseline. Following the practice in [31], baselines using CaffeNet and ResNet-50 are fine-tuned with the default parameter settings except that the output dimension of the last FC layer is set to the number of training identities. The CaffeNet Baseline is trained for 60 epochs with a learning rate of 0.001 and then for another 20 epochs with a learning rate of 0.0001. The ResNet Baseline is trained for 60 epochs with learning rate initialized at 0.001 and reduced by 10 on 25 and 50 epochs. During testing, the FC6 or FC7 descriptor of CaffeNet and the Pool5 or FC descriptor of ResNet-50 are used for feature representation.

On Market-1501, CaffeNet and Resnet-50 achieves rank-1 accuracy of 55.3% (73.8%) with the FC6 (Pool5) descriptor, which is consistent with the results in [31].

Detailed settings. CaffeNet-backed SVDNet takes 25 RRIs to reach final convergence. The 1st to the 24th RRI contains 2000×2 iterations separately, with batch size set to 64 and learning rate fixed at 0.001. The last Restraint training contains 8000 iterations. The learning rate is initialized with 0.001 and divided by 10 after 5000 iterations. ResNet-backed SVDNet takes 7 RRIs to reach approximate convergence. Each RRI contains 8000×2 iterations, with batch size set to 32. Learning rate is divided by 10 after 5000 iterations. The initial learning rate for the 1st to the 3rd RRI is set to 0.001, and the initial learning rate for the

Models & Features	dim	Market-1501				CUHK03				Duke			
		R-1	R-5	R-10	mAP	R-1	R-5	R-10	mAP	R-1	R-5	R-10	mAP
Baseline(C) FC6	4096	55.3	75.8	81.9	30.4	38.6	66.4	76.8	45.0	46.9	63.2	69.2	28.3
Baseline(C) FC7	4096	54.6	75.5	81.3	30.3	42.2	70.2	80.4	48.6	45.9	62.0	69.7	27.1
SVDNet(C) FC6	4096	80.5	91.7	94.7	55.9	68.5	90.2	95.0	73.3	67.6	80.5	85.7	45.8
SVDNet(C) FC7	1024	79.0	91.3	94.2	54.6	66.0	89.4	93.8	71.1	66.7	80.5	85.1	44.4
Baseline(R) Pool5	2048	73.8	87.6	91.3	47.9	66.2	87.2	93.2	71.1	65.5	78.5	82.5	44.1
Baseline(R) FC	N	71.1	85.0	90.0	46.0	64.6	89.4	95.0	70.0	60.6	76.0	80.9	40.4
SVDNet(R) Pool5	2048	82.3	92.3	95.2	62.1	81.8	95.2	97.2	84.8	76.7	86.4	89.9	56.8
SVDNet(R) FC	1024	81.4	91.9	94.5	61.2	81.2	95.2	98.2	84.5	75.9	86.4	89.5	56.3

Table 2. Comparison of the proposed method with baselines. C: CaffeNet. R: ResNet-50. In ResNet Baseline, the FC layer denotes the last FC layer, and its output dimension N changes with the number of training identities, *i.e.*, 751 on Market1501, 1160 on CUHK03 and 762 on Duke. In ResNet-backed SVDNet, the FC layer denotes the Eigen Layer, its output dimension is set to 1024.

rest RRIs is set to 0.0001.

The dimension of Eigen Layer’s output is set to be 1024 in all models, yet the influence of this hyper-parameter is to be analyzed in Section 4.4. The reason of using different times of RRIs for different backbones is to be illustrated in Section 4.5.

4.3. Performance Evaluation

The effectiveness of SVDNet. We comprehensively evaluate the proposed SVDNet on all the three re-ID benchmarks. The overall results are shown in Table 2.

The improvements achieved on both backbones are significant: When using CaffeNet as the backbone, the Rank-1 accuracy on Market-1501 rises from 55.3% to 80.5%, and the mAP rises from 30.4% to 55.9%. On CUHK03 (Duke) dataset, the Rank-1 accuracy rises by +26.3% (+20.7%), and the mAP rises by +24.7% (+17.5%). When using ResNet as the backbone, the Rank-1 accuracy rises by +8.4%, +15.6% and +11.2% respectively on Market-1501, CUHK03 and Duke dataset. The mAP rises by +14.2%, +13.7% and +12.7% correspondingly.

Some other valuable phenomena can be observed as well. The proposed method presents a property of steady: on all the 3 datasets, almost all the best performance is achieved using the Eigen Layer’s input feature (*i.e.*, FC6 on SVDNet(C) and pool5 on SVDNet(R)), while the baseline’s optimal layer for feature representation varies. However, Eigen Layer’s output feature is still valued considering that its lower dimension reduces the computing cost for matching, *e.g.*, on Market1501, using the 1024-d SVDNet(C)’s FC7 feature achieves the Rank-1 accuracy of 79.0%, only 1.5% lower than using the 4096-d FC6 feature.

Comparison with state of the art.

We compare SVDNet with the state-of-the-art methods. Comparisons on Market-1501 and CUHK03 are shown in Table 3. Comparing with already published papers, SVDNet achieves competitive performance. We report **rank-1 = 82.3%, mAP = 62.1% on Market-1501, and**

Methods	Market-1501		CUHK03	
	rank-1	mAP	rank-1	mAP
LOMO+XQDA[13]	43.8	22.2	44.6	51.5
CAN[15]	48.2	24.4	63.1	-
SCSP[4]	51.9	26.4	-	-
Null Space[28]	55.4	29.9	54.7	-
DNS[28]	61.0	35.6	54.7	-
LSTM Siamese[23]	61.6	35.3	57.3	46.3
MLAPG[14]	-	-	58.0	-
Gated SCNN[22]	65.9	39.6	61.8	51.3
ReRank (C) [35]	61.3	46.8	58.5	64.7
ReRank (R) [35]	77.1	63.6	64.0	69.3
PIE (A)* [29]	65.7	41.1	62.6	67.9
PIE (R)* [29]	79.3	56.0	67.1	71.3
SOMAnet (VGG)* [2]	73.9	47.9	72.4	-
DLCE (C)* [33]	62.1	39.6	59.8	65.8
DLCE (R)* [33]	79.5	59.9	83.4	86.4
Transfer (G)* [9]	83.7	65.5	84.1	-
SVDNet(C)	80.5	55.9	68.5	73.3
SVDNet(R,1024d)	82.3	62.1	81.8	84.8

Table 3. Comparison with state of the art on Market-1501 (single query) and CUHK03. * denotes unpublished ArXiv papers. Different base networks are annotated. C: CaffeNet, R: ResNet-50, A: AlexNet, G: GoogleNet [21]. The best, second and third highest results are in blue, red and green, respectively.

rank-1 = 81.8%, mAP = 84.8% on CUHK03. The re-ranking method [35] is higher than ours in mAP on Market-1501, because re-ranking exploits the relationship among the gallery images and results in a high recall. We speculate that this re-ranking method will also bring improvement for SVDNet. Comparing with the unpublished Arxiv papers, (some of) our numbers are slightly lower than [9] and [33]. Both works [9] and [33] combine the verification and classification losses, and we will investigate into integrating this strategy into SVDNet.

Moreover, our method’s performance on simple CNN

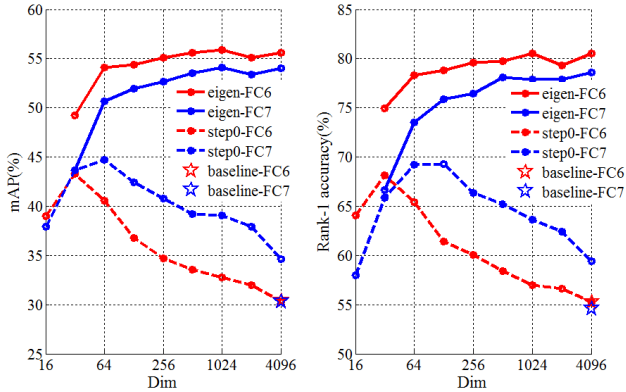


Figure 3. CaffeNet-backed SVDNet

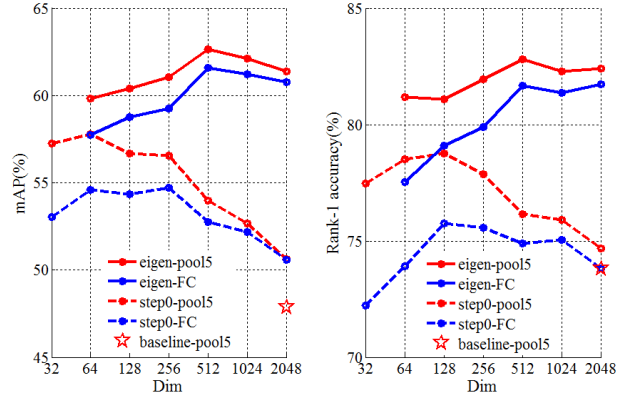


Figure 4. ResNet-backed SVDNet

Methods	rank-1	mAP
BoW+kissme [30]	25.1	12.2
LOMO+XQDA [13]	30.8	17.0
Baseline (R) [31]	65.2	45.0
GAN (R) [34]	67.7	47.1
SVDNet (C)	67.6	45.8
SVDNet (R)	76.7	56.8

Table 4. Comparison with the state of the art on Duke. Rank-1 accuracy (%) and mAP (%) are shown.

architecture is impressive. On Market-1501, CaffeNet-backed SVDNet achieves 80.5% rank-1 accuracy and 55.9% mAP, exceeding other CaffeNet-based methods by a large margin. Additionally, we achieve 79.7% and 77.4% rank-1 accuracy separately on VGGNet and Tiny CaffeNet. On CUHK03, CaffeNet-backed SVDNet even exceeds other ResNet-based methods except for DLCE(R). This observation implies that our method can achieve acceptable performance with high computing effectiveness.

Comparisons on Duke are summarized in Table 4. Relatively fewer results are reported because this dataset has only been recently benchmarked. This paper reports **rank-1 = 76.7%**, **mAP = 56.8%**, which is higher than the several competing methods including a recent GAN approach [34].

4.4. Dimension comparison

We train SVDNet with Eigen layer’s output dimension set various. Results for CaffeNet and ResNet backbone models are drawn in Fig. 3 and Fig. 4 respectively.

It can be observed that the dimension of Eigen Layer’s output significantly influences the immediate performance (*i.e.*, without enforcing orthogonality to W). The approximate regularity is that the performance rises as the dimension drops. In the 16-d (32-d) case in CaffeNet (ResNet)-backbone models, it seems to defy the regularity. However, we observe that in the two cases, the models fail

to converge to a comparable level with others: the final training loss remains above 0.5 and the identification accuracy on training set remains lower than 100%, indicating that the models are incapable of fitting the training data.

After enforcing orthogonality to the weight matrix, the influence of Eigen Layer’s output feature dimension shows a different trend. The performance gradually increases with the dimension until saturation. ResNet-backed SVDNet achieves the highest performance on the 512-d setting, with 83.1% rank-1 accuracy and 62.6% mAP, which might be due to random disturbance compared with the 1024-d and 2048-d settings.

4.5. RRI boosting procedure

This experiment reveals how the performance changes after each Restraint training as well as Relaxation training, and how SVDNet reaches the final performance step by step. We set both Restraint phase and Relaxation phase in one iteration to contain 25 epochs. The output dimension of Eigen Layer is set to 2048. Exhaustively we test all the intermediate models, with results shown in Fig. 5, from which three conclusions can be drawn.

First, Rank-1 accuracy curve presents an alternating rhythm of “increase and decrease” echoing the Restraint and Relaxation Iteration: When W is frozen to maintain orthogonality during Restraint training, the performance increases, implying a boosting to feature representation’s discriminability. Then during Relaxation training, W is free to get updated, and the performance stagnates or even decreases slightly. However, the total trend is increase. Second, it is reliable to use $S(W)$ indicating the degree of orthogonality as convergence criteria. Third, when backbone on ResNet, RRI converges much faster than that backbone on CaffeNet.

4.6. Comparison of decorrelating methods

In Section 3.3, when exploring the potential ways of decorrelating Eigen Layer’s weight vectors, we prove that

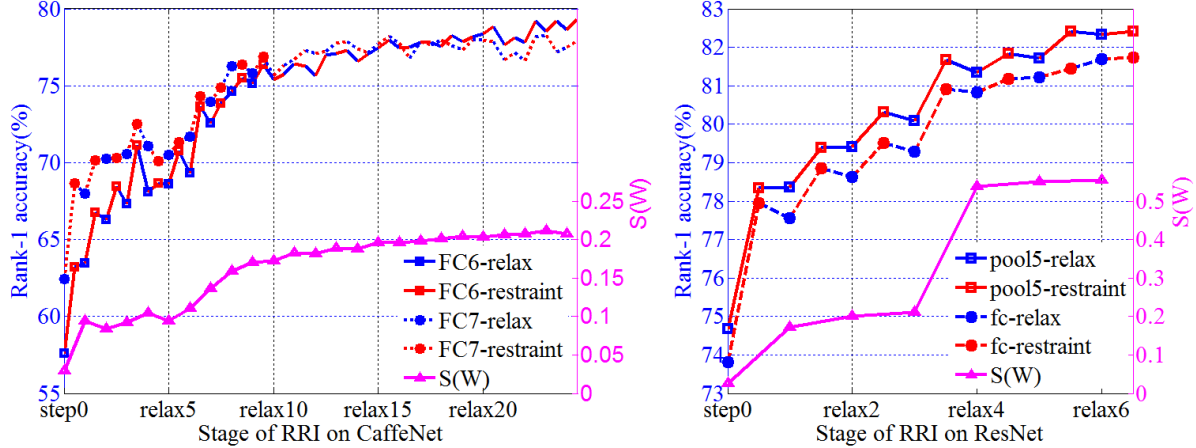


Figure 5. Performance of each intermediate model during RRI. CaffeNet-backed SVDNet takes about 25 RRIs to converge. Testing results of models before Relaxation-10 is marked with dot. Refer to Eq. 2 for definition of $S(W)$. Here it is used as the convergence criteria for RRI. ResNet-backed SVDNet takes about 7 RRIs to converge. $S(W)$ curve shows a jump on the relax4 point because the initial training rate for Relaxation 4 is reduced to 0.0001.

Methods	<i>Orig</i>	<i>US</i>	<i>U</i>	UV^T	<i>QD</i>
FC6(C)	57.0	80.5	76.2	57.4	58.8
FC7(C)	63.6	79.0	75.8	62.7	63.2
pool5(R)	75.9	82.3	80.9	76.5	77.9
FC(R)	75.1	81.4	80.2	74.8	77.3

Table 5. Comparison of decorrelating methods. Rank-1 accuracy (%) on Market-1501 is shown. Dimension of Eigen Layer’s output is set to 1024. C: CaffeNet. R: ResNet-50

only the proposed method of replacing $W = USV^T$ with US maintains the discriminability of Eigen Layer’s output feature, while other 3 methods all cause performance degradation by some extent. This experiment compares the final performance using 4 different decorrelating methods marked with US , U , UV^T and QD as detailed in Section 3.3.

Results are shown in Table 5. It can be observed that the proposed decorrelating method US achieves the highest performance, followed by the U , QD and the UV^T method. Moreover, the UV^T method actually does not offer any observable improvement compared with the *Orig*. This experiment demonstrates that not only the orthogonality itself, but also the approach to decorrelating weight vectors, is vital for SVDNet.

5. Conclusion

In this paper, SVDNet is introduced for representation learning in pedestrian retrieval, or re-identification. Decorrelation is enforced among the projection vectors in the weight matrix of the FC layer. Through iterations of

“restraint and relaxation”, we show that the extent of vector correlation is gradually reduced. In this process, the re-ID performance undergoes iterative “increase and decrease”, and finally reaches a stable accuracy. Due to the linear independence of the weight vectors, the learned embedding better suits the retrieval task under the Euclidean distance. Significant improvement is observed on the Market-1501, CUHK03 and Duke datasets, and the re-ID accuracy is competitive with the state of the art.

In the future, we will explore the combination of SVDNet with several competitive methods including [9, 33]. We will also extend its application to other retrieval problems such as instance and face retrieval.

References

- [1] E. Ahmed, M. J. Jones, and T. K. Marks. An improved deep learning architecture for person re-identification. In *CVPR*, 2015. 2
- [2] I. B. Barbosa, M. Cristani, B. Caputo, A. Rognhaugen, and T. Theoharis. Looking beyond appearances: Synthetic training data for deep cnns in re-identification. *arXiv preprint arXiv:1701.03153*, 2017. 6
- [3] T. Chan, K. Jia, S. Gao, J. Lu, Z. Zeng, and Y. Ma. Pcanet: A simple deep learning baseline for image classification? *IEEE Trans. Image Processing*, 24(12):5017–5032, 2015. 2
- [4] D. Chen, Z. Yuan, B. Chen, and N. Zheng. Similarity learning with spatial constraints for person re-identification. In *CVPR*, pages 1268–1277, 2016. 6
- [5] D. Cheng, Y. Gong, S. Zhou, J. Wang, and N. Zheng. Person re-identification by multi-channel parts-based cnn with improved triplet loss function. In *Proceedings of the IEEE Conference on Computer Vision and Pattern Recognition*, pages 1335–1344, 2016. 2

- [6] D. S. Cheng, M. Cristani, M. Stoppa, L. Bazzani, and V. Murino. Custom pictorial structures for re-identification. In *Bmvc*, 2011. 2
- [7] E. L. Denton, W. Zaremba, J. Bruna, Y. LeCun, and R. Fergus. Exploiting linear structure within convolutional networks for efficient evaluation. In *NIPS*, 2014. 2
- [8] P. Felzenszwalb, D. McAllester, and D. Ramanan. A discriminatively trained, multiscale, deformable part model. In *Computer Vision and Pattern Recognition, 2008. CVPR 2008. IEEE Conference on*, pages 1–8. IEEE, 2008. 5
- [9] M. Geng, Y. Wang, T. Xiang, and Y. Tian. Deep transfer learning for person re-identification. *arXiv preprint arXiv:1611.05244*, 2016. 1, 2, 6, 8
- [10] K. He, X. Zhang, S. Ren, and J. Sun. Deep residual learning for image recognition. In *CVPR*, 2016. 1, 5
- [11] A. Krizhevsky, I. Sutskever, and G. E. Hinton. Imagenet classification with deep convolutional neural networks. In *NIPS*, 2012. 1, 5
- [12] W. Li, R. Zhao, T. Xiao, and X. Wang. Deepreid: Deep filter pairing neural network for person re-identification. In *CVPR*, 2014. 2, 5
- [13] S. Liao, Y. Hu, X. Zhu, and S. Z. Li. Person re-identification by local maximal occurrence representation and metric learning. In *CVPR*, 2015. 6, 7
- [14] S. Liao and S. Z. Li. Efficient PSD constrained asymmetric metric learning for person re-identification. In *ICCV*, 2015. 6
- [15] H. Liu, J. Feng, M. Qi, J. Jiang, and S. Yan. End-to-end comparative attention networks for person re-identification. *arXiv preprint arXiv:1606.04404*, 2016. 6
- [16] E. Ristani, F. Solera, R. Zou, R. Cucchiara, and C. Tomasi. Performance measures and a data set for multi-target, multi-camera tracking. In *European Conference on Computer Vision*, pages 17–35. Springer, 2016. 1
- [17] E. Ristani, F. Solera, R. Zou, R. Cucchiara, and C. Tomasi. Performance measures and a data set for multi-target, multi-camera tracking. In *European Conference on Computer Vision workshop on Benchmarking Multi-Target Tracking*, 2016. 5
- [18] K. Simonyan and A. Zisserman. Very deep convolutional networks for large-scale image recognition. *arXiv preprint arXiv:1409.1556*, 2014. 5
- [19] C. Su, S. Zhang, J. Xing, W. Gao, and Q. Tian. Deep attributes driven multi-camera person re-identification. In *European Conference on Computer Vision*, pages 475–491. Springer, 2016. 2
- [20] Y. Sun, Y. Chen, X. Wang, and X. Tang. Deep learning face representation by joint identification-verification. In *Advances in neural information processing systems*, pages 1988–1996, 2014. 2
- [21] C. Szegedy, W. Liu, Y. Jia, P. Sermanet, S. Reed, D. Anguelov, D. Erhan, V. Vanhoucke, and A. Rabinovich. Going deeper with convolutions. In *Proceedings of the IEEE Conference on Computer Vision and Pattern Recognition*, pages 1–9, 2015. 6
- [22] R. R. Variator, M. Haloi, and G. Wang. Gated siamese convolutional neural network architecture for human re-identification. In *ECCV*, 2016. 2, 6
- [23] R. R. Variator, B. Shuai, J. Lu, D. Xu, and G. Wang. A siamese long short-term memory architecture for human re-identification. In *ECCV*, 2016. 2, 6
- [24] T. Xiao, H. Li, W. Ouyang, and X. Wang. Learning deep feature representations with domain guided dropout for person re-identification. In *CVPR*, 2016. 1, 2
- [25] D. Xie, J. Xiong, and S. Pu. All you need is beyond a good init: Exploring better solution for training extremely deep convolutional neural networks with orthonormality and modulation. In *CVPR*, 2017. 2
- [26] J. Xue, J. Li, and Y. Gong. Restructuring of deep neural network acoustic models with singular value decomposition. In *Interspeech*, 2013. 2
- [27] D. Yi, Z. Lei, S. Liao, and S. Z. Li. Deep metric learning for person re-identification. In *ICPR*, 2014. 2
- [28] L. Zhang, T. Xiang, and S. Gong. Learning a discriminative null space for person re-identification. In *CVPR*, 2016. 6
- [29] L. Zheng, Y. Huang, H. Lu, and Y. Yang. Pose invariant embedding for deep person re-identification. *arXiv preprint arXiv:1701.07732*, 2017. 1, 2, 6
- [30] L. Zheng, L. Shen, L. Tian, S. Wang, J. Wang, and Q. Tian. Scalable person re-identification: A benchmark. In *ICCV*, 2015. 5, 7
- [31] L. Zheng, Y. Yang, and A. G. Hauptmann. Person re-identification: Past, present and future. *arXiv preprint arXiv:1610.02984*, 2016. 1, 2, 5, 7
- [32] L. Zheng, H. Zhang, S. Sun, M. Chandraker, and Q. Tian. Person re-identification in the wild. In *CVPR*, 2017. 2
- [33] Z. Zheng, L. Zheng, and Y. Yang. A discriminatively learned CNN embedding for person re-identification. *arXiv preprint arXiv:1611.05666*, 2016. 2, 6, 8
- [34] Z. Zheng, L. Zheng, and Y. Yang. Unlabeled samples generated by gan improve the person re-identification baseline in vitro. *arXiv preprint arXiv:1701.07717*, 2017. 5, 7
- [35] Z. Zhong, L. Zheng, D. Cao, and S. Li. Re-ranking person re-identification with k-reciprocal encoding. In *CVPR*, 2017. 6